doi:10.1246/cl.2011.1316
1316 Published on the web November 26, 2011

Highlight Review

Arylethynylanthraquinone and Bis(arylethynyl)anthraquinone: Strong Donor–Acceptor Interaction and Proton-induced Cyclization to Form Pyrylium and Dipyrylium Salts

Ryota Sakamoto, Koya Prabhakara Rao, and Hiroshi Nishihara*

(Received October 18, 2011; CL-118012)

Abstract

In this account we describe ethynylene-conjugated arylethynylanthraquinone (**ArAq**) and bis(arylethynyl)anthraquinone (**Ar$_2$Aq**) which possess ferrocene, triarylamine, platinadithiolene complex, *p*-methoxybenzene, *p*-methylbenzene, *m*-methylbenzene, and benzene as electron-donating arenes (**Ar**), and anthraquinone (**Aq**) as an electron acceptor. This series of compounds features donor–acceptor (**D–A**) interactions: (1) Expression of intramolecular charge-transfer (ICT) transitions; (2) flexible single crystal networks constructed by intermolecular **D–A** π–π stacking, which undergo guest-induced reversible crystal-to-crystal transformations. In addition, **ArAq** and **Ar$_2$Aq** experience proton-induced cyclization so as to produce pyrylium and dipyrylium salts. These salts feature further expanded π-conjugation and stronger **D–A** interaction: (1) More red-shifted ICT transitions and narrower HOMO–LUMO gaps; (2) bright fluorescence; (3) valence tautomerism (VT); (4) unique reactivities.

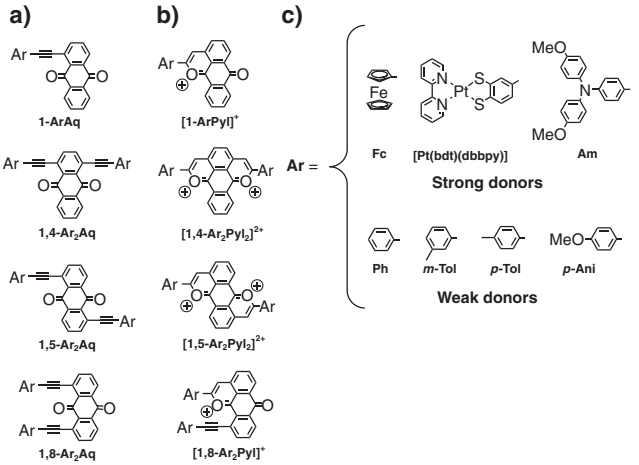

Scheme 1. a) Arylethynylanthraquinone and bis(arylethynyl)-anthraquinone. b) Pyrylium and dipyrylium salts. c) Electron-donating arenes used in this study.

♦ Introduction

Donor–acceptor (**D–A**) systems have gained increasing attention from a wide range of research fields. For example, isolated and **D** and **A** molecules can be incorporated into single crystals, which exhibit intermolecular **D–A** interaction and accompanying valuable physical properties, such as neutral–ionic transition,[1] formation of charge-transfer (CT) complexes,[2–4] ferromagnetism,[2] strong visible–NIR light absorption,[3] high electric conductivity,[4] and so on.

Recent progress in synthetic chemistry has made it possible to synthesize more elaborated **D–A** systems. Fukuzumi and coworkers have designed and synthesized various kinds of **D–A** multiads where the **D** and **A** components are tethered with one another via covalent bonds, so as to realize thermal and photoinduced charge separation systems with long lifetimes.[5] **D–A** interaction has been also exploited in rotaxanic supramolecular systems in order to embody electrochemically-switchable bistability.[6]

D–A, **D–A–D**, and **A–D–A** molecules where their components are connected in π-conjugated fashions are also promising functional materials. For example, they feature strong absorptions in the visible and NIR regions, which are assigned to intramolecular charge-transfer (ICT) transitions through the π connectors: their large absorptivities often lead to high fluorescent quantum yields.[7] In addition, it has been demonstrated that these types of molecules possess excellent nonlinear optical (NLO) properties, which can be utilized in various applications.[8] π-Conjugated **D–A** molecules have proven to undergo valence tautomerism (VT),[9] which affords molecular bistability with drastic changes in optical and magnetic properties.[10]

We have developed various kinds of π-conjugated **D–A** and **D–A–D** compounds:[11–15] Especially, in this decade we have keenly investigated arylethynylanthraquinone (**ArAq**) and bis(arylethynyl)anthraquinone (**Ar$_2$Aq**) in which electron-donating aryl groups (**Ar**, Scheme 1c) are connected to electron-withdrawing anthraquinone (**Aq**) via ethynylene linkers (Scheme 1a).[15] We prepared **1-ArAq** alone as the **ArAq** family, whereas the **Ar$_2$Aq** family includes **1,4-Ar$_2$Aq**, **1,5-Ar$_2$Aq**, and **1,8-Ar$_2$Aq**. This review treats the comprehensive chemistry of this series of **D–A** and **D–A–D** systems: synthesis, expression of intramolecular CT transitions, and formation of soft porous crystals woven by intermolecular **D–A** interaction. In addition, proton-induced intramolecular cyclization of **ArAq** and **Ar$_2$Aq** to afford pyrylium and dipyrylium cations (**[1-ArPyl]$^+$**, **[1,4-Ar$_2$Pyl$_2$]$^{2+}$**, **[1,5-Ar$_2$Pyl$_2$]$^{2+}$**, and **[1,8-Ar$_2$Pyl]$^+$**, Scheme 1b),

*Dr. Ryota Sakamoto, Dr. Koya Prabhakara Rao, and Prof. Hiroshi Nishihara**
Department of Chemistry, Graduate School of Science, The University of Tokyo,
7-3-1 Hongo, Bunkyo-ku, Tokyo 113-0033
E-mail: nisihara@chem.s.u-tokyo.ac.jp

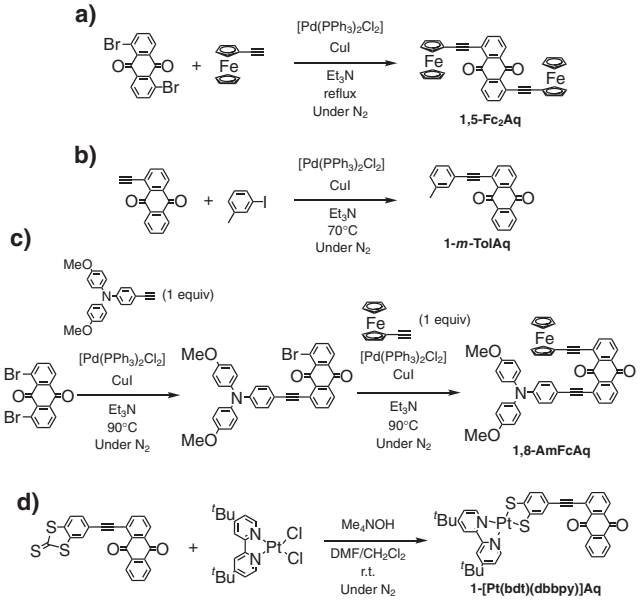

Scheme 2. Representative synthetic methods for arylethynylanthraquinone and bis(arylethynyl)anthraquinone.

respectively, and resultant expansion of the π conjugation, intensification of the intramolecular **D–A** interaction, photoluminescence, VT phenomena, and unique reactivities, are also described.

♦ Synthesis of ArAq and Ar_2Aq

Halogenated anthraquinone can be converted to the corresponding **ArAq** and **Ar_2Aq** in good yields by means of a Sonogashira–Hagihara cross coupling protocol using arylacetylene (Scheme 2a). Another access is the Sonogashira–Hagihara cross coupling between ethynylanthraquinone and aryl halide (Scheme 2b). These facile synthetic methods greatly helped us to synthesize a wide range of isomers with various **Ar**. Heterodonor molecules are practically unavailable in this series of systems except for the 1,8-isomer: stepwise Sonogashira–Hagihara reactions with triarylaminoacetylene, and then ferrocenylacetylene resulted in heterodonor **1,8-AmFcAq** (Scheme 2c). We note that the reversion of the order of arylacetylene did not afford **1,8-AmFcAq**: We assume that the bulkiness of **Am** significantly decelerates the second Sonogashira–Hagihara reaction. **1-[Pt(bdt)(dbbpy)]Aq** was obtained by the deprotection of the anthraquinone-conjugated dithiolato ligand, followed by complexation with a Pt source (Scheme 2d).

♦ Absorption Spectra of ArAq and Ar_2Aq

The **ArAq** and **Ar_2Aq** families with strong donor **Ar** sites such as **Fc** and **Am** exhibit characteristic electronic bands in the visible region, assignable to ICT transitions from the donor **Ar** to the acceptor **Aq** (Figure 1: **1-FcAq**: $\lambda_{max} = 514$ nm, $\varepsilon_{max} = 1800\,M^{-1}\,cm^{-1}$; **1-AmAq**: $\lambda_{max} = 486$ nm, $\varepsilon_{max} = 4600\,M^{-1}\,cm^{-1}$). This strongly manifests the existence of intramolecular **D–A** interaction. We note that **1-[Pt(bdt)(dbbpy)]Aq** should possess ICT bands in the visible region, though the existence is obscured by a strong visible absorption intrinsic to the dithiolato-diimine–Pt(II) type of complexes.[16]

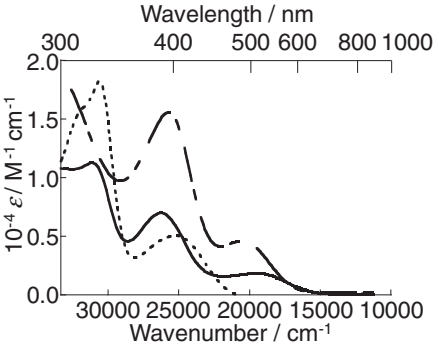

Figure 1. UV–vis spectra of **1-FcAq** (solid line), **1-AmAq** (dashed line), and **1-*p*-TolAq** (dotted line) in dichloromethane.

♦ Guest-induced Crystal-to-crystal Transitions in 1,4-Fc_2Aq

Porous materials that can construct nanometer-sized spaces have attracted much attention because of their potential use in applications such as selected gas adsorption,[17] heterogeneous catalysts,[18] and molecular recognition.[19] Beyond the conventional porous materials, such as activated carbon and zeolite, recent attention has been concentrated on porous coordination polymers (PCPs), which are also known as metal–organic frameworks (MOFs).[20] PCPs feature infinite network backbones comprising metal ions and organic ligands, which are mutually connected by coordination bonds. PCPs often have nanometer-sized pores, so that they can encapsulate guest molecules such as gaseous and solvent molecules. One of the virtues of PCPs over other types of porous materials is the regularity and designability of their porous structures, which are precisely determined by the shape and size of the organic ligands, and the coordination mode of the metal centers.

Intensive recent efforts have made it possible to construct "third generation" PCPs, which can change their crystal structures reversibly in response to the injection and ejection of guest molecules, and also, chemical and physical outer stimuli.[20p] Such "soft" crystals lead to, for example, selective adsorption and desorption of guest molecules. There are still limitations to fabricate third generation PCPs because of their robust structures based on coordination bonds.

We anticipated that π–π stacking triggered by the intermolecular **D–A** interaction of **1,4-Fc_2Aq** in the crystalline state, which should be more flexible than coordination bonds in PCPs, could be exploited in creating soft crystals featuring reversible transformations of the porous crystal structures upon guest uptake and discharge.

1,4-Fc_2Aq was significantly easy to crystallize: for example, recrystallization from dichloromethane–hexane at 263 K resulted in huge crystals (e.g., $25 \times 1 \times 1\,mm^3$) within a week (Figure 2a). In addition, different crystallization conditions (e.g., poor solvents, rich solvents, and temperatures) afforded different shapes of crystals, the structures of which were all verified by single-crystal X-ray diffraction (XRD) analysis. This

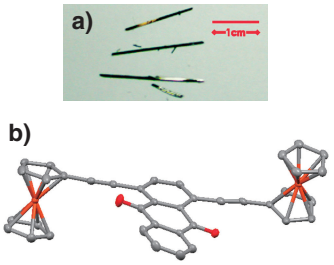

Figure 2. a) Huge single crystals of **α-1,4-Fc$_2$Aq·CH$_2$Cl$_2$**; b) ORTEP drawing of the **1,4-Fc$_2$Aq** molecule in a single crystal of **α-1,4-Fc$_2$Aq·CH$_2$Cl$_2$**; C: gray, O: red, Fe: orange. Hydrogen atoms and disordered guest molecules are omitted for clarity.

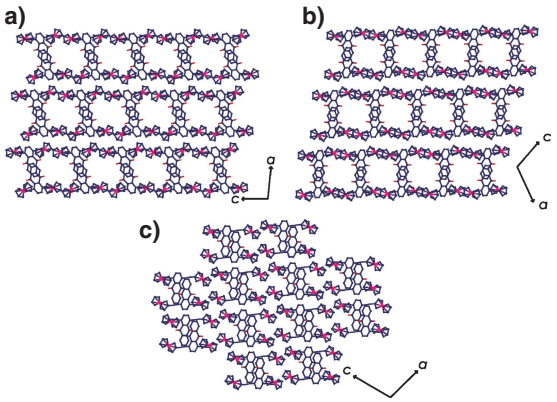

Figure 3. Crystal structures along the *b* axis: a) **α-1,4-Fc$_2$Aq·CH$_2$Cl$_2$**; b) **β-1,4-Fc$_2$Aq·CH$_2$Cl$_2$**; c) guest-free **1,4-Fc$_2$Aq**. Hydrogen atoms and disordered guest molecules are omitted for clarity.

series of analyses clarified that the formulae of these crystals could be represented as **1,4-Fc$_2$Aq·G**, where **G** is a solvent molecule as a guest.

An ORTEP drawing of the **1,4-Fc$_2$Aq** molecule in **α-1,4-Fc$_2$Aq·CH$_2$Cl$_2$** is shown in Figure 2b, which possesses the "*anti*" configuration with respect to the two ferrocene units. Its crystal structure along the *b* axis is shown in Figure 3a. **α-1,4-Fc$_2$Aq·CH$_2$Cl$_2$** has ultrasmall pores with a size of 5.7 Å × 3.5 Å along the *b* axis, where dichloromethane guest molecules are stored in the pores with a ratio between the host and guest of 1:1. An infinite one-dimensional columnar structure is formed along the *b* axis by an alternating arrangement of the π-conjugated spacer and a π–π stacking interaction between electron-donating **Fc** and electron-withdrawing **Aq** (Figure 4a). The planes defined by **Aq**, ethynylene linker, and cyclopentadienyl (Cp) ring form angles of ca. 45° with the *b* axis. Two types of columns are almost perpendicular to each other, and are arranged alternately to construct the porous framework. Most of the guest-encapsulated crystals belong to this type. In this class of crystals, polymorphology was observed with small guest solvents (e.g., dichloromethane, chloroform, and tetrachloromethane): Figure 3b shows another crystal structure of **1,4-Fc$_2$Aq** with dichloromethane, **β-1,4-Fc$_2$Aq·CH$_2$Cl$_2$**. Small guest molecules tend to be extremely disordered. On the other hand, only one crystal structure was formed when **G** was a larger guest molecule such as THF, trichloroethylene, and hexane.

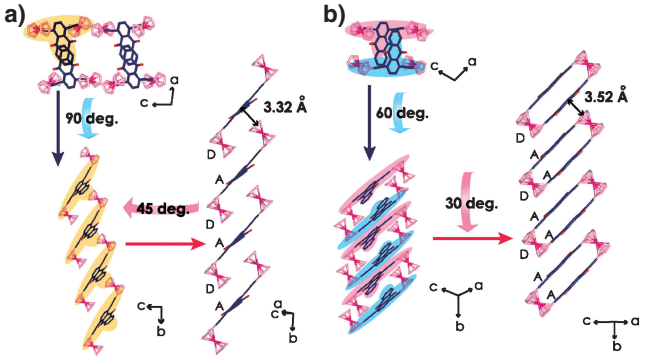

Figure 4. One-dimensional columnar structures: a) in **1,4-Fc$_2$Aq·X**; b) in guest-free **1,4-Fc$_2$Aq**.

Recrystallization of **1,4-Fc$_2$Aq** at 293 K from *o*-dichlorobenzene–hexane afforded crystals without pores and guest solvent molecules (Figure 3c). The solvent-free form also feature a columnar structure; however, the "*syn*" conformation with respect to the two **Fc** units in a **1,4-Fc$_2$Aq** molecule gives rise to pairs of **1,4-Fc$_2$Aq** in the crystal, and a **D–A–A** type of π–π stacking (Figure 4b).

There is a manifest tendency that the **D–A** π–π stacking distance is shorter in **1,4-Fc$_2$Aq·G** than in the guest-free **1,4-Fc$_2$Aq**, as shown in Figure 4. This fact indicates the guest-holding crystal structures reap stabilization from the stronger **D–A** interaction. In fact, **1,4-Fc$_2$Aq·THF** is more stabilized than guest-free **1,4-Fc$_2$Aq** ($\Delta G = -32$ kJ mol^{-1}, estimated from differential scanning calorimetry). Furthermore, the activation energy for the desorption of the guest molecules, E_{de}, for **1,4-Fc$_2$Aq·THF** was also estimated by recording thermogravimetric curves at various heating rates,[21] to afford E_{de} of 127 kJ mol^{-1}.

This series of crystallographic studies indicates that the crystal systems based on **1,4-Fc$_2$Aq** are flexible, and have the possibility of showing reversible guest adsorption and desorption. The crystal-to-crystal transformations of **1,4-Fc$_2$Aq** upon introduction and removal of guest solvents were surveyed by variable-temperature X-ray powder diffraction (VT-XRPD). For this measurement, we prepared a vacuum-sealed 1 mmϕ glass capillary tube containing a 0.5 mmϕ capillary filled with frozen THF and a 0.5 mmϕ capillary packed with guest-free **1,4-Fc$_2$Aq** powder (Figure 5). After three hours at room temperature, the XRPD pattern of the sample completely changed from guest-free **1,4-Fc$_2$Aq** (Figure 5(i)) to guest-charged **1,4-Fc$_2$Aq·THF** (Figure 5(ii)). By setting the temperature of the guest (T_g) at 90 K and that of the sample (T_s) at 400 K, the sample in the **1,4-Fc$_2$Aq·THF** state released the guest THF molecules and recovered the XRPD pattern of guest-free **1,4-Fc$_2$Aq** (Figure 5(iii)). On the other hand, when the capillary was refilled with THF vapor by increasing T_g, THF was adsorbed to the host again, so that the XRPD pattern arising from **1,4-Fc$_2$Aq·THF** was recovered (Figures 5(iv)–5(vii)). Similar crystal-to-crystal transformations by reversible guest adsorption and desorption were also observed with chloroform as the guest.

The rate of crystal-to-crystal transformation from guest-free **1,4-Fc$_2$Aq** to **1,4-Fc$_2$Aq·THF** was also estimated by VT-XRPD. In this measurement, at T_s and T_g of 300 K, the guest adsorption abruptly started at 2 min after the introduction of the guest vapor, and the transformation was completed within 5 min. In the first

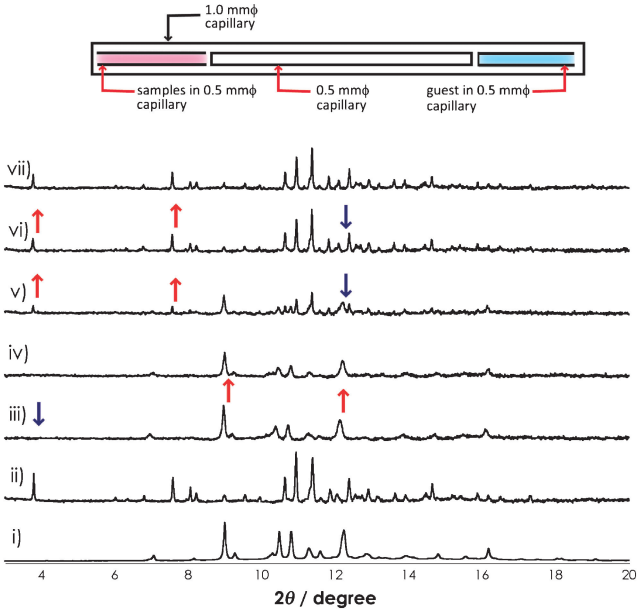

Figure 5. VT-XRPD patterns: (i) Solvent-free **1,4-Fc$_2$Aq** at room temperature; (ii) $T_s = 350$ K, $T_g = 90$ K; (iii) $T_s = 400$ K, $T_g = 90$ K; (iv) $T_s = 300$ K, $T_g = 200$ K; (v) $T_s = 300$ K, $T_g = 300$ K; (vi) $T_s = 300$ K, $T_g = 350$ K; and (vii) $T_s = 300$ K, $T_g = 400$ K.

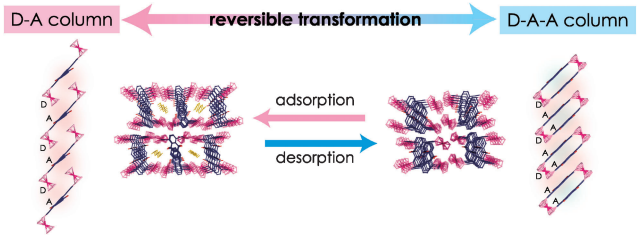

Scheme 3. Schematic illustration of the reversible crystal-to-crystal transformations upon guest adsorption and desorption in **1,4-Fc$_2$Aq**.

2 min, the guest vapor pressure was not enough to induce the guest inclusion. Such a gating phenomenon is usually observed in crystal systems where relatively large structural changes are needed for crystal-to-crystal transformations.[17a,22]

This series of VT-XRPD results indicates that solvent-free **1,4-Fc$_2$Aq** undergoes rapid and reversible crystal-to-crystal transformations between the **1,4-Fc$_2$Aq·THF** form (Scheme 3). Such immediate transformations are particularly remarkable.[23] These features result from the flexibility of the crystal structures rendered by the intermolecular **D–A** π–π stacking, which is weaker than other chemical bonds.

♦ *Formation of Pyrylium Salts Induced by Protonation*

1-FcAq exhibited a significant color change upon addition of trifluoromethanesulfonic acid (TfOH): We had first regarded this reaction as a protonation to the anthraquinone, and a successive conformation change to a fulvene–cumulene structure, which had been in a VT equilibrium as shown in Scheme 4a; however, due to the low crystallinity of the resultant species, we had not been able to obtain the critical proof on its structure at the early stage. This work reached a turning point by employing bis(trifluoromethanesulfon)imide (TFSIH) as a proton source: we could obtained single crystals of the resultant material, the quality of which was good enough to clarify the structure (Figure 6). It was of great surprise that one of the carbonyl groups participated in cyclization with the ethynylene linker, to form **[1-FcPyl](TFSI)** with a pyrylium ring. **[1-FcPyl](TFSI)** featured a highly planar tetracyclic structure including the pyrylium ring. The counter anion was exchangeable to BF_4^- and PF_6^- by recrystallization with additives of *n*-Bu_4BF_4 and *n*-Bu_4PF_6, respectively. ^{1}H NMR spectra of **[1-FcPyl](TFSI)** in acetonitrile-d_3 exhibited a characteristic singlet peak at 8.23 ppm, assignable to the solitary proton of the pyrylium ring. The IR spectrum of **1-FcAq** in a KBr pellet exhibited a C≡C stretching vibration at 2219 cm^{-1}, whereas it disappeared in that of **[1-FcPyl](TFSI)**. Consistently, the ^{13}C NMR spectra of **[1-ArAq](TFSI)** in acetonitrile-d_3 lost signals around 85–100 ppm, ascribable to the ethynylene linker. All **1-ArAq** shown in Scheme 1 underwent the same type of annulation reactions, although the reaction rate was highly dependent on **Ar**. For example, an addition of 1.5 equivalents of TFSIH to a 0.1 mM solution of **1-FcAq** in dichloromethane resulted in a rapid conversion (within 10 s) to **[1-FcPyl]$^+$**, whereas at this condition **1-*p*-TolAq** did not at all show the cyclocondensation: more concentrated TFSIH was needed to afford **[1-*p*-TolPyl]$^+$**. Thus, **1-ArAq** with a stronger donor was more prone to cyclize. In addition, more polar aprotic media, such as 1,2-dichloroethane, proved to accelerate the pyrylium generation. In reference to the previous pyrylium synthesis by Swager and co-workers (i.e., acid-induced cyclization in *o*-alkynyldimethylbenzamide, ethyl benzoate, benzaldehyde, and benzophenone)[24] and our experimental results enumerated

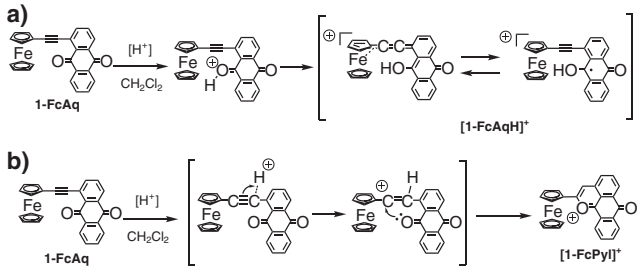

Scheme 4. a) Initially proposed acid-response of **1-FcAq**. b) Plausible scheme for the generation of **[1-FcPyl]$^+$**.

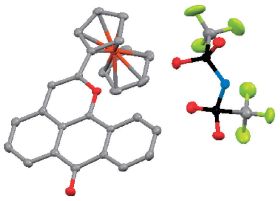

Figure 6. ORTEP drawing of **[1-FcPyl](TFSI)**; C: gray, O: red, Fe: orange, S: black, N: blue, F: yellow. Hydrogen atoms are omitted for clarity.

above, we suggest a plausible reaction mechanism in Scheme 4b. An electrophilic attack of a proton at the β carbon of the ethynylene linker gives rise to a carbocation intermediate where the positive charge is localized on the α carbon. This intermediate is expected to be stabilized by **Ar** with strong donor ability, and also, by polar solvents, which might lead to the acceleration of the reaction rate under these conditions. Then the carbocation intermediate undergoes the nucleophilic cyclization with the neighboring carbonyl group.

♦ *Formation of Pyrylium Salts Induced by Double Protonation*

Intramolecular double cyclization is a valuable tool for the creation of functional molecules that feature high planarity, fused-ring structure, and intensive π-conjugation.[25] In response to the cyclization of **1-ArAq** to generate the corresponding pyrylium cations **[1-ArPyl]$^+$**, we expected that the **1,4-**, **1,5-**, and **1,8-Ar$_2$Aq** underwent intramolecular double cyclization to generate the corresponding dipyrylium salts, which featured more developed π-conjugation than singly cyclized **[1-ArPyl]$^+$**.

1,4-Fc$_2$Aq readily gave the corresponding dipyrylium cation, **[1,4-Fc$_2$Pyl$_2$]$^{2+}$**, upon treatment with five equivalents of TFSIH in dichloromethane in 30 min (Scheme 5a). Similarly, **1,4-Am$_2$Aq** was quantitatively converted to **[1,4-Am$_2$Pyl$_2$]$^{2+}$** under the same conditions. On the other hand, **1,4-Ar$_2$Aq** with weak donors (i.e., **Ar** = **Ph**, ***p*-Tol**, and ***p*-Ani**) gave monoannulated compounds. To complete the double cyclization in these compounds, more harsh conditions were essential: 1,2-dichloromethane as a more polar solvent, TfOH as a more acidic proton source, and longer reaction time. The sluggish double-cyclization reaction in **1,4-Ar$_2$Aq** with weak donors might come from the second annulation step, because the cationic monopyrylium ring in the intermediates should be a strong electron-withdrawing group (Scheme 5a). Among the **[1,4-Ar$_2$Pyl$_2$]$^{2+}$** series, only **[1,4-Fc$_2$Pyl$_2$](BF$_4$)$_2$** provided single crystals worth analyzing in XRD analysis. Figure 7a shows its ORTEP drawing, manifesting the quintuply fused planar dipyrylium framework. Distinctive changes were observed in IR spectroscopy: the spectrum of **1,4-Fc$_2$Aq** in KBr pellets featured stretching vibrations of C≡C (2200 cm^{-1}) and C=O (1665 cm^{-1}), whereas those of **[1,4-Fc$_2$Pyl$_2$]X$_2$** (**X** = TFSI, TfO, and BF$_4$) lost these signals due to the participation of these bonds in the double cyclization.

1,5-Fc$_2$Aq and **1,5-Am$_2$Aq** also immediately reacted with TFSIH in dichloromethane, to afford **[1,5-Fc$_2$Pyl$_2$]$^{2+}$** and **[1,5-Am$_2$Pyl$_2$]$^{2+}$** (Scheme 5b). These dipyrylium salts gave single crystals of low quality, therefore only preliminary XRD analysis was conducted to reveal a planar pentacyclic dipyrylium skeleton. The stretching vibrations of C≡C and C=O diminished upon the conversion from **1,5-Ar$_2$Aq** to **[1,5-Ar$_2$Pyl$_2$]$^{2+}$** in IR spectra. As far as **1,4-Ar$_2$Aq** and **1,5-Ar$_2$Aq** are compared, we could not find a difference in the reactivity against protons. We note that monocyclized **[1,5-Am$_2$Pyl](TFSI)** was isolated by the control of the equivalents of TFSIH.

1,8-Fc$_2$Aq and **1,8-Am$_2$Aq** underwent a proton-induced pyrylium formation contrastive to the 1,4- and 1,5-families (Scheme 5c): only a single annulation was observed in these compounds, which was revealed by means of single-crystal X-ray structure analysis for **[1,8-Fc$_2$Pyl](BF$_4$)** (Scheme 5c and Figure 7b). This is rationalized by the fact that the unreacted

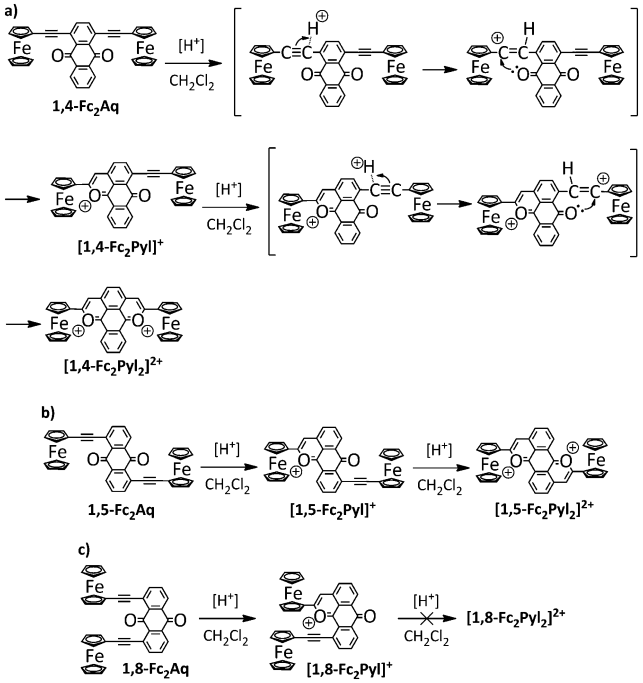

Scheme 5. a) Stepwise double cyclization in **1,4-Fc$_2$Aq** with a plausible reaction mechanism; b) stepwise double cyclization in **1,5-Fc$_2$Aq**; c) single cyclization in **1,8-Fc$_2$Aq**.

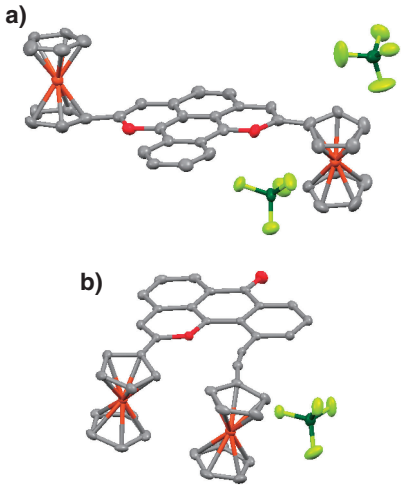

Figure 7. ORTEP drawings; a) **[1,4-Fc$_2$Pyl$_2$](BF$_4$)$_2$**. b) **[1,8-Fc$_2$Pyl](BF$_4$)**; C: gray, O: red, Fe: orange, B: green, F: yellow. Hydrogen atoms are omitted for clarity.

ethynylene is spatially too distant from the residual carbonyl group to take part in the second annulation.

♦ *Expanded π-Conjugation of Pyrylium and Dipyrylium Salts*

The resultant pyrylium and dipyrylium salts were expected to gain intensive expansion on π-conjugation. We confirmed this expectation by means of UV–vis–NIR spectroscopy, density

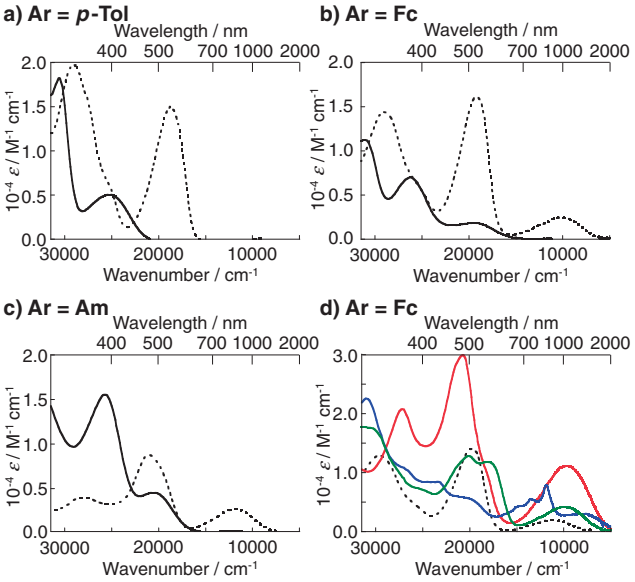

Figure 8. UV–vis–NIR spectra of **1-ArAq** (solid line) and **[1-ArPyl](TFSI)** (dotted line) in dichloromethane: a) **Ar** = ***p*-Tol**; b) **Ar** = **Fc**; c) **Ar** = **Am**; d) UV–vis–NIR spectra of **[1-FcPyl](TFSI)** (black dotted line), **[1,4-Fc_2Pyl_2](TFSI)$_2$** (red solid line), **[1,5-Fc_2Pyl_2](TFSI)$_2$** (blue solid line), and **[1,8-Fc_2Pyl](TFSI)** (green solid line) in acetonitrile.

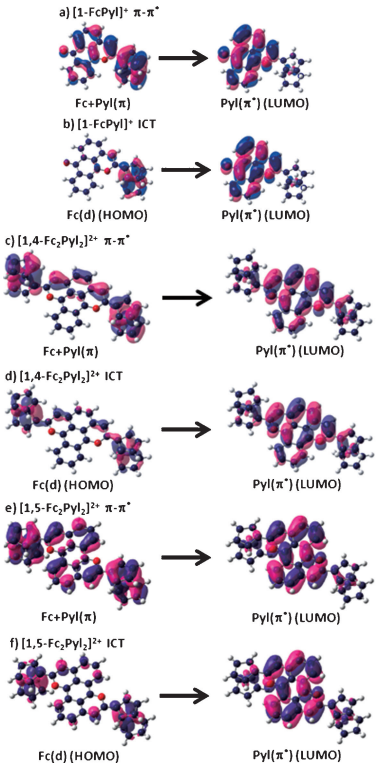

Figure 9. Chief transitions estimated by TDDFT calculations: a) In the π–π^* band of **[1-FcPyl]**$^+$; b) in the ICT band of **[1-FcPyl]**$^+$; c) in the π–π^* band of **[1,4-Fc_2Pyl_2]**$^{2+}$; d) in the ICT band of **[1,4-Fc_2Pyl_2]**$^{2+}$; e) in the π–π^* band of **[1,5-Fc_2Pyl_2]**$^{2+}$; f) in the ICT band of **[1,5-Fc_2Pyl_2]**$^{2+}$.

functional theory (DFT) and time-dependent DFT (TDDFT) calculations, and electrochemical measurements.

Figures 8a–8c show UV–vis–NIR spectral changes of **1-ArAq** (**Ar** = ***p*-Tol**, **Fc**, and **Am**) upon the formation of the pyrylium salts. An emergence of intense absorptions around 500 nm was observed as a common change (**[1-*p*-TolPyl]**$^+$: $\lambda_{max} = 531$ nm, $\varepsilon_{max} = 15000\,M^{-1}\,cm^{-1}$; **[1-FcPyl]**$^+$: $\lambda_{max} = 520$ nm, $\varepsilon_{max} = 16000\,M^{-1}\,cm^{-1}$; **[1-AmPyl]**$^+$: $\lambda_{max} = 474$ nm, $\varepsilon_{max} = 8800\,M^{-1}\,cm^{-1}$). According to the TDDFT calculations, this series of new bands was assigned to π–π^* transitions mostly localized on the tetracyclic pyrylium plane (Figure 9a): the occupied π orbitals contain a contribution from **Ar**. In **[1-ArPyl]**$^+$ with weak donors, this π–π^* band is the HOMO–LUMO transition, and thereby is responsible for the lowest photoexcited state. On the other hand, those with strong donors featured broad NIR absorptions (**[1-FcPyl]**$^+$: $\lambda_{max} = 992$ nm, $\varepsilon_{max} = 2500\,M^{-1}\,cm^{-1}$; **[1-AmPyl]**$^+$: $\lambda_{max} = 846$ nm, $\varepsilon_{max} = 2700\,M^{-1}\,cm^{-1}$): the TDDFT calculations assigned them to ICT transitions from the donors, **Fc**(d) and **Am**(n), to the π^* orbital of the tetracyclic pyrylium moiety (Figure 9b). We note that **{1-[Pt(bdt)(dbbpy)]Pyl}**$^+$ possessed a more intense, broad, and asymmetric ICT band than **[1-FcPyl]**$^+$ and **[1-AmPyl]**$^+$. This feature arises from the fact that **[Pt(bdt)(dbbpy)]** has two platinadithiole(π) orbitals, which underlie the HOMO and HOMO−1, and participate in two ICT bands independently. The drastic red shift of the ICT bands upon the cyclization manifests that the HOMO–LUMO gap is significantly contracted, and more intense **D–A** interaction is acquired by this transformation.

Figure 8d shows an overlay of the UV–vis–NIR spectra of **[1-FcPyl]**$^+$, **[1,4-Fc_2Pyl_2]**$^{2+}$, **[1,5-Fc_2Pyl_2]**$^{2+}$, and **[1,8-Fc_2Pyl]**$^+$ in acetonitrile, all of which feature both π–π^* and ICT bands (Figures 9c–9f). **[1,8-Fc_2Pyl]**$^+$ displayed a spectrum relatively similar to that of **[1-FcPyl]**$^+$, which is consistent with the fact that both compounds underwent the single annulation. On the other hand, **[1,4-Fc_2Pyl_2]**$^{2+}$ and **[1,5-Fc_2Pyl_2]**$^{2+}$ experienced more profound spectral changes: the former significantly gained intensity of each band. On the other hand, the latter featured the most red-shifted π–π^* and ICT bands. These spectroscopic characteristics in **[1,4-Fc_2Pyl_2]**$^{2+}$ and **[1,5-Fc_2Pyl_2]**$^{2+}$ indicate that the double cyclization reaction worked quite well for further expansion of the π conjugation with respect to the dipyrylium pentacyclic plane: in fact, the TDDFT calculations demonstrated that the π^* orbitals of these compounds spread over the whole pentacyclic dipyrylium rings (Figures 9c–9f).

The narrowing of the HOMO–LUMO gap was also confirmed by means of electrochemical measurements. Figure 10 shows the cyclic voltammograms of **1-AmAq** and **[1-AmPyl](TFSI)** in 0.1 M Bu_4NClO_4–dichloromethane. **1-AmAq** exhibited reversible one-electron oxidation and reduction, which stem from the **Am**(n) and **Aq**(π^*), respectively. On the other hand, **[1-AmPyl](TFSI)** underwent a reversible one-electron oxidation, and two reversible one-electron reductions: the former is derived from the **Am**(n), while the latter originate from the **Pyl**(π^*). Noteworthy is that the HOMO–LUMO gap gets significantly small upon the cyclization (Figure 11a). Figures 11b and 11c also depict the redox potentials of **1,4-Am_2Aq** and **1,5-Am_2Aq** before and after the double annula-

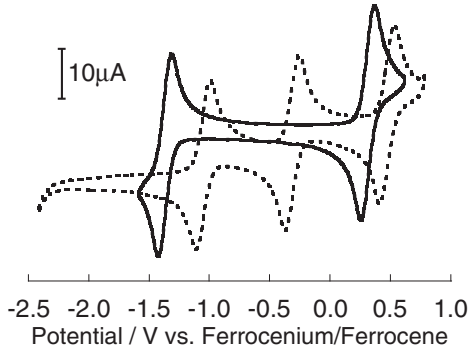

Figure 10. Cyclic voltammograms of **1-AmAq** (solid line) and **[1-AmPyl](TFSI)** (dotted line) in 0.1 M Bu_4NClO_4–dichloromethane at a sweep rate of 100 mV s^{-1}.

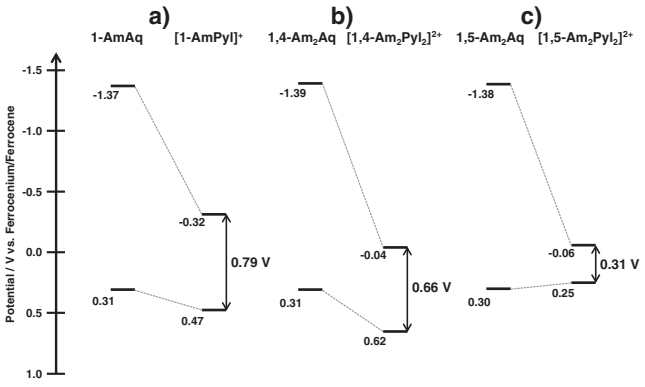

Figure 11. Schematic potential diagrams for **1-AmAq**, **1,4-Am_2Aq**, and **1,5-Am_2Aq** before and after the cyclization estimated from the redox potentials measured by means of cyclic voltammetry.

tion. **[1,4-Am_2Pyl_2]$^{2+}$** and **[1,5-Am_2Pyl_2]$^{2+}$** feature narrower HOMO–LUMO gaps than **[1-AmPyl]$^+$**, which can be ascribable to the further expansion of the π conjugation upon the formation of the dipyrylium cations: especially, **[1,5-Am_2Pyl_2]$^{2+}$** possesses the narrowest HOMO–LUMO gap.

♦ Fluorescence

[1-*p*-TolPyl](TFSI) ($\lambda_{max} = 650$ nm, $\phi_F = 0.09$, Figure 12), **[1-*m*-TolPyl](TFSI)** ($\lambda_{max} = 628$ nm, $\phi_F = 0.20$), and **[1-PhPyl](TFSI)** ($\lambda_{max} = 611$ nm, $\phi_F = 0.19$) exhibited broad and unstructured fluorescence with large Stokes shifts in dichloromethane at room temperature upon excitation of the π–π^* band. Fluorescence with such features is often observed in pyrylium salts,[26] though, λ_{max} of our molecules is significantly red-shifted due to the developed π-conjugated electronic structure. Detectable fluorescence was not observed in **[1-ArPyl](TFSI)** with strong donors.

♦ Valence Tautomerism

The authors expected that the significant narrowing of the HOMO–LUMO gap (Figure 11), and resultant intensification of the **D–A** interaction upon the proton-induced pyrylium and

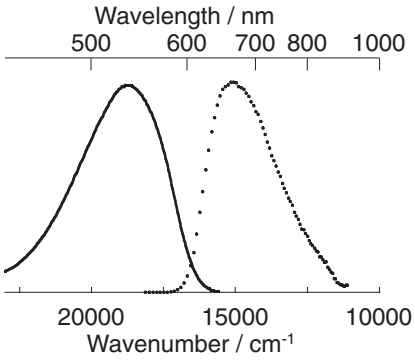

Figure 12. Normalized absorption (solid) and fluorescence (dotted) spectra of **[1-*p*-TolPyl](TFSI)** in dichloromethane upon excitation of the π–π^* band.

dipyrylium formation could induce VT upon intermolecular electron transfers.

[1-FcPyl]X (**X** = **TFSI**, **PF_6**, and **BF_4**) was diamagnetic in solution, and had nothing to do with VT. On the other hand, it showed a drastic response to temperature in the crystalline solid state. Variable-temperature Mössbauer spectroscopy at a range of 12–300 K clarified that the molar ratio between the Fe(II) and Fe(III) states was dependent on temperature in the samples of **X** = **TFSI** and **PF_6** (Figures 13a and 13b): At low temperatures the Fe(II) state was dominant, whereas the Fe(III) state was more favorable at high temperatures. Therefore, these salts were in VT as shown in Scheme 6. On the other hand, **[1-FcPyl]BF_4** was independent of temperature with respect to the molar ratio, exhibiting only the Fe(II) state (Figure 13c). These three pyrylium salts were brought under review by means of single-crystal XRD analysis. A definitive difference lay on the dihedral angle between the **Pyl** plane and the Cp ring bonding to **Pyl**: The BF_4 salt possessed a dihedral angle of 11.25(15)°, which was greater than those of the TFSI (6.63(12)°) and PF_6 (9.55(15)°) salts. The smaller dihedral angle could afford the more intense intramolecular **D–A** communication, and as a result could promote an electron transfer from **Fc** to **Pyl**. Furthermore, the distortion of the **Pyl** plane was more significant in the BF_4 salt. This structural strain might cause a destabilization of the LUMO level, leading to the energetically unfavored Fe(III) state. This series of VT phenomena in **[1-FcPyl](TFSI)** and **[1-FcPyl]-(PF_6)**, however, was not reflected in SQUID measurements: Paramagnetic susceptibility was not at all observed at any temperature in both salts. We attributed this to intramolecular antiferromagnetic interaction.

(1-[Pt(bdt)(dbbpy)]Pyl)(TFSI) was NMR silent, which was in sharp contrast to the cases of diamagnetic **[1-FcPyl]-(TFSI)** and **[1-AmPyl](TFSI)** in solution. EPR measurement in solution demonstrated that **{1-[Pt(bdt)(dbbpy)]Pyl}(TFSI)** contained a small portion of paramagnetic species (0.3–1.0%), and a SQUID measurement in the solid state was also consistent with this result. We ascribed the origin of this paramagnetism to its valence tautomer generated by an intramolecular electron transfer (Scheme 7). This VT should be induced by the stronger donor ability of the **[Pt(bdt)(dbbpy)]** than **Fc** and **Am**.[16f]

As shown in Figure 11, the double cyclization in **1,4-Ar_2Aq** and **1,5-Ar_2Aq** caused more significant π-expansion and narrower HOMO–LUMO gaps, than the single annulation in

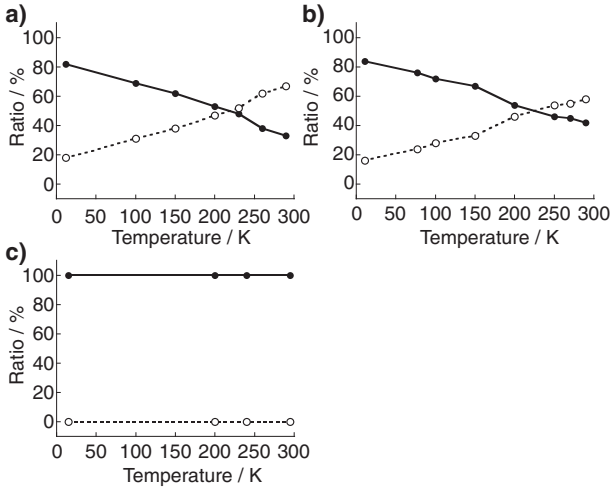

Figure 13. Temperature dependence of the molar ratio between Fe(II) (black dots and solid lines) and Fe(III) (white dots and dotted lines) species in the crystalline solid state calculated by means of Mössbauer spectroscopy: a) **[1-FcPyl](TFSI)**; b) **[1-FcPyl](PF$_6$)**; c) **[1-FcPyl](BF$_4$)**.

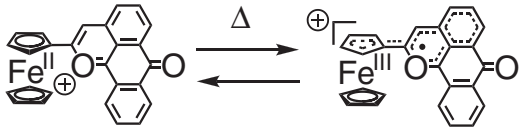

Scheme 6. VT phenomenon in **[1-FcPyl]**$^+$. In the Fe(III) state, the two spins localized at the **Fc** and **Pyl** moieties are antiferromagnetically coupled in an intramolecular fashion.

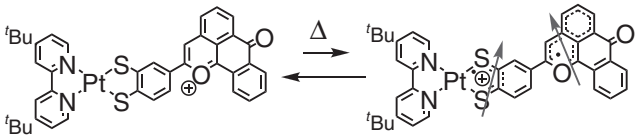

Scheme 7. VT phenomenon in **{1-[Pt(bdt)(dbbpy)]Pyl}**$^+$. The gray arrow indicates an electron spin.

1-ArAq; therefore, more profound VT was expected for **[1,4-Ar$_2$Pyl$_2$]X$_2$** and **[1,5-Ar$_2$Pyl$_2$]X$_2$**. Doubly cyclized **[1,4-Am$_2$Pyl$_2$](TFSI)$_2$** was found to show broadened signals in ^{1}H NMR, and **[1,5-Am$_2$Pyl$_2$](TFSI)$_2$** were found to be NMR silent. This series of results suggested that **[1,4-Am$_2$Pyl$_2$](TFSI)$_2$** and **[1,5-Am$_2$Pyl$_2$](TFSI)$_2$** were in equilibrium with the corresponding paramagnetic valence tautomers, which were generated by one-electron and two-electron transfers from **Am** to **Pyl** (Scheme 8). In fact, the EPR spectra of **[1,4-Am$_2$Pyl$_2$](TFSI)$_2$** and **[1,5-Am$_2$Pyl$_2$](TFSI)$_2$** in dichloromethane displayed their paramagnetic nature: the molar spin densities were calculated to be 2% for **[1,4-Am$_2$Pyl$_2$](TFSI)$_2$** and 30% for **[1,5-Am$_2$Pyl$_2$](TFSI)$_2$** per molecule at room temperature. In particular, the spectrum of **[1,5-Am$_2$Pyl$_2$](TFSI)$_2$** at room temperature featured a 27-fold split (Figure 14), which was well reproduced by a simulation presuming that the two spins generated by the two-electron transfer were localized on the two **Am** sites, and hyperfine structures were afforded by their N and H atoms. The

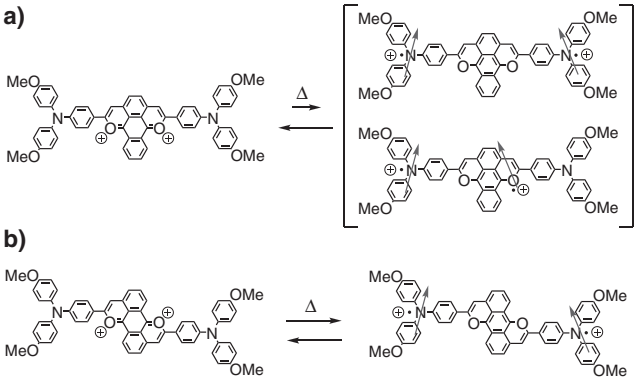

Scheme 8. VT phenomena: a) in **[1,4-Am$_2$Pyl$_2$]**$^{2+}$; b) in **[1,5-Am$_2$Pyl$_2$]**$^{2+}$.

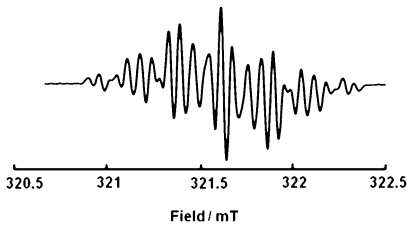

Figure 14. EPR spectrum of **[1,5-Am$_2$Pyl$_2$](TFSI)$_2$** in dichloromethane at room temperature.

magnetic susceptibility measurements in the solid state using a SQUID magnetometer also outputted the spin densities consistent with those by EPR spectroscopy. These results indicated that the spin density was distributed over the two triarylamine moieties as a result of the single or double electron transfer from the electron-donating triarylamine moieties to the highly electron-accepting pentacyclic dipyrylium skeleton (Scheme 8). The substitution position of the **Am** significantly impacted the spin density, which was consistent with the HOMO–LUMO gap shown in Figure 11.

♦ *Reactivity of the Pyrylium and Dipyrylium Salts*

Upon treatment with MeOH or MeONa, **[1-ArPyl]**$^+$ underwent a reaction that was accompanied by the loss of the π–π^* band. For those with strong donors, the CT band also disappeared (Figure 15a). Exploiting various NMR techniques (^{1}H, ^{13}C, ^{1}H–^{1}H COSY, HMQC, and HMBC), we finally identified the resultant product for **[1-*p*-TolPyl]**$^+$ as a methoxide adduct, **1-*p*-TolPyl-OMe** (Scheme 9a). Surprisingly, **1-ArPyl-OMe** could experience an acid-induced backward reaction, to regenerate **[1-ArPyl]**$^+$ (Scheme 9a). This was proven by the quantitative UV–vis–NIR spectral recovery (Figure 15b). In combination with the fluorescent ability of **[1-*p*-TolPyl]**$^+$, we performed a reversible switching of fluorescence triggered by acid (TFSIH) and base (MeONa) (Scheme 10).

Dipyrylium **[1,5-Am$_2$Pyl$_2$]**$^{2+}$ did not show any responses to MeOH and MeONa (Scheme 9c), however, its structural isomer **[1,4-Am$_2$Pyl$_2$]**$^{2+}$ reacted with these chemicals, to afford **1,4-Am$_2$(Pyl-OMe)$_2$** (Scheme 9b). This was confirmed by high-

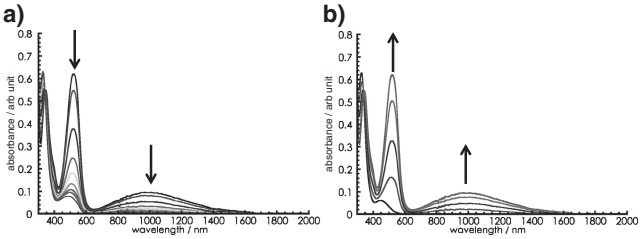

Figure 15. a) UV–vis–NIR spectra of **[1-FcPyl]**$^{+}$ upon a stepwise addition of methanol in dichloromethane; b) UV–vis–NIR spectra of **1-FcPyl-OMe** upon a stepwise addition of TFSIH in dichloromethane.

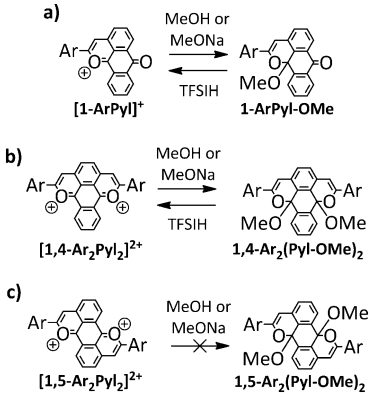

Scheme 9. a) Reversible conversion between **[1-ArPyl]**$^{+}$ and **1-ArPyl-OMe** upon addition of MeOH or MeONa, and TFSIH; b) quasi-reversible conversion between **[1,4-Ar$_2$Pyl$_2$]**$^{2+}$ and **1,4-Ar$_2$(Pyl-OMe)$_2$** upon addition of MeOH or MeONa, and TFSIH; c) inertness of **[1,5-Ar$_2$Pyl$_2$]**$^{2+}$ against MeOH or MeONa.

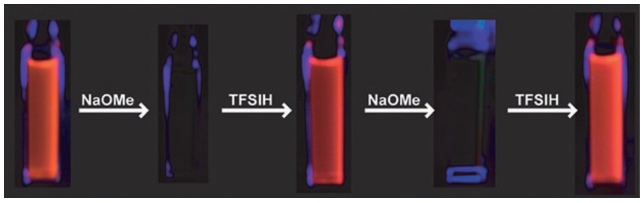

Scheme 10. Acid–base response of **[1-*p*-TolPyl]**$^{+}$ in dichloromethane. Each photo was taken with irradiation of 360 nm UV light.

resolution ESI-TOF-MS and UV–vis–NIR spectroscopy. **1,4-Am$_2$(Pyl-OMe)$_2$** quasi-reversibly reverted to **1,4-Am$_2$Pyl$_2$** by an addition of TFSIH (Scheme 9b).

Another important and interesting reactivity in **[1,4-Am$_2$Pyl$_2$]**$^{2+}$ and **[1,5-Am$_2$Pyl$_2$]**$^{2+}$ was that neutral compounds could be generated by a two-electron reduction. The neutral compounds **[1,4-Am$_2$Pyl$_2$]**^{0} and **[1,5-Am$_2$Pyl$_2$]**^{0} were prepared by treating **[1,4-Am$_2$Pyl$_2$](TFSI)$_2$** and **[1,5-Am$_2$Pyl$_2$](TFSI)$_2$** with lithium tetracyanoquinodimethane, Li(TCNQ). Single-crystal X-ray analyses disclosed that these neutral molecules maintained the planar pentacyclic backbone of the dipyrylium salts (Figure 16). The difference between **[1,4-Am$_2$Pyl$_2$]**^{0} and **[1,5-Am$_2$Pyl$_2$]**^{0} lay in the fact that the former was more stable against moisture, oxygen, and so on. Apart from the **Am** moieties, **[1,4-Am$_2$Pyl$_2$]**$^{2+}$ and **[1,5-Am$_2$Pyl$_2$]**$^{2+}$ have electronic structures identical to benzo[*e*]pyrene and perylene with 20π electrons. On the other hand, **[1,4-Am$_2$Pyl$_2$]**^{0} and **[1,5-Am$_2$Pyl$_2$]**^{0} can be regarded as 22π-electron molecules, which meet the aromatic "$4n + 2$ rule." Therefore, this result opens a new area of heteroatom-containing polycyclic aromatic hydrocarbons (PAHs).

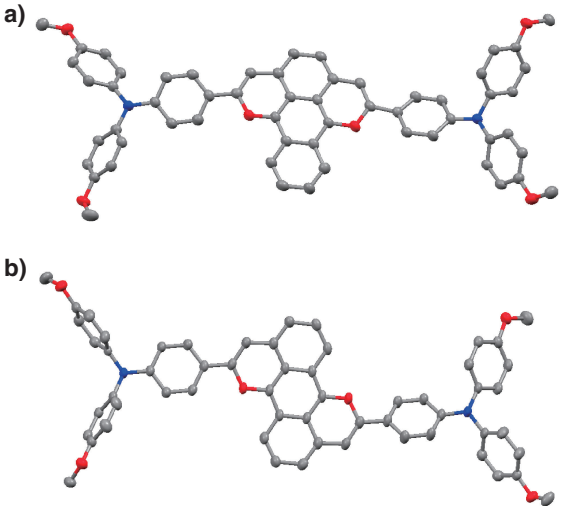

Figure 16. ORTEP drawings: a) **[1,4-Am$_2$Pyl$_2$]**^{0}; b) **[1,5-Am$_2$Pyl$_2$]**^{0}; C: grey, O: red, N: blue. Hydrogen atoms are omitted for clarity.

♦ Summary

In this review, we addressed a comprehensive explanation of the **D–A 1-ArAq**, and the **D–A–D 1,4-Ar$_2$Aq**, **1,5-Ar$_2$Aq**, and **1,8-Ar$_2$Aq**. A brief synthetic procedure of these compounds with a Sonogashira–Hagihara coupling protocol made it possible to synthesize molecules with a wide range of **Ar**. The existence of intramolecular **D–A** interaction was confirmed by the expression of CT transitions from **Ar** to **Aq** with strong donor moieties. **1,4-Fc$_2$Aq** embodied intermolecular **D–A** interaction as π–π stacking in the crystal phase: This interaction played a vital role in the realization of a porous crystalline material that featured crystal-to-crystal transformations in response to guest molecules. **1-ArAq**, **1,4-Ar$_2$Aq**, **1,5-Ar$_2$Aq**, and **1,8-Ar$_2$Aq** exhibited peculiar proton responses, which was identified by means of single-crystal XRD as the formation of the corresponding pyrylium and dipyrylium salts **[1-ArPyl]X**, **[1,4-Ar$_2$Pyl$_2$]X$_2$**, **[1,5-Ar$_2$Pyl$_2$]X$_2$**, and **[1,8-Ar$_2$Pyl]X** upon single or double cyclization, rather than as mere protonation to the **Aq** moiety. UV–vis–NIR spectroscopy and electrochemical measurements disclosed that the pyrylium and dipyrylium salts featured more expanded π conjugation, significant lowering of the LUMO levels, and narrower HOMO–LUMO gaps than the parent compounds: these impacts were greater in the doubly-annulated compounds. For the sake of the small HOMO–LUMO gaps, parts of the pyrylium and dipyrylium salts underwent VT among one-electron and two-electron transferred species from the donor(s) to the acceptor. When **Ar** was a weak donor, **[1-ArPyl]X** brightly emitted fluorescence around 600–850 nm.

[1-ArPyl]X and **[1,4-Ar$_2$Pyl$_2$]X$_2$** were subject to methanol or sodium methoxide, giving rise to neutral methoxide adducts **1-ArPyl-OMe** and **1,4-Ar$_2$(Pyl-OMe)$_2$**. This addition was reversed by treatment with acid, to afford the original pyrylium and dipyrylium salts. **[1,4-Am$_2$Pyl$_2$]X$_2$** and **[1,5-Am$_2$Pyl$_2$]X$_2$** could be reduced by two electrons to afford neutral species **[1,4-Am$_2$Pyl$_2$]^0** and **[1,5-Am$_2$Pyl$_2$]^0**: The parent dipyrylium salts had electronic structures identical to those of 20π benzo[*e*]pyrene and perylene, and the neutral compounds could be regarded as the first 22π analogs of these PAHs.

The authors are grateful to Grants-in-Aid from MEXT of Japan (Nos. 20245013 and 21108002, Area 2107, Coordination Programming) and the Global COE Program for Chemistry Innovation for financial support.

References

1 a) J. B. Torrance, A. Girlando, J. J. Mayerle, J. I. Crowley, V. Y. Lee, P. Batail, S. J. LaPlaca, *Phys. Rev. Lett.* **1981**, *47*, 1747. b) J. J. Mayerle, J. B. Torrance, J. I. Crowley, *Acta Crystallogr., Sect. B: Struct. Crystallogr. Cryst. Chem.* **1979**, *35*, 2988.

2 a) A. Alberola, E. Coronado, J. R. Galán-Mascarós, C. Giménez-Saiz, C. J. Gómez-García, *J. Am. Chem. Soc.* **2003**, *125*, 10774. b) K. Mukai, S. Jinno, Y. Shimobe, N. Azuma, M. Taniguchi, Y. Misaki, K. Tanaka, K. Inoue, Y. Hosokoshi, *J. Mater. Chem.* **2003**, *13*, 1614. c) T. Matsumoto, T. Kominami, K. Ueda, T. Sugimoto, T. Tada, S. Noguchi, H. Yoshino, K. Murata, M. Shiro, E.-i. Negishi, N. Toyota, S. Endo, K. Takahashi, *Inorg. Chem.* **2002**, *41*, 4763. d) G. Wang, C. Slebodnick, R. J. Butcher, M. C. Tam, T. D. Crawford, G. T. Yee, *J. Am. Chem. Soc.* **2004**, *126*, 16890. e) H. Nakajima, M. Katsuhara, M. Ashizawa, T. Kawamoto, T. Mori, *Inorg. Chem.* **2004**, *43*, 6075.

3 a) M. Chollet, L. Guerin, N. Uchida, S. Fukaya, H. Shimoda, T. Ishikawa, K. Matsuda, T. Hasegawa, A. Ota, H. Yamochi, G. Saito, R. Tazaki, S.-i. Adachi, S.-y. Koshihara, *Science* **2005**, *307*, 86. b) H. Nishihara, M. Kurashina, K. Aramaki, K. Kubo, *Synth. Met.* **1999**, *101*, 457.

4 a) J. Ferraris, D. O. Cowan, V. Walatka, Jr., J. H. Perlstein, *J. Am. Chem. Soc.* **1973**, *95*, 948. b) G. Saito, H. Sasaki, T. Aoki, Y. Yoshida, A. Otsuka, H. Yamochi, O. O. Drozdova, K. Yakushi, H. Kitagawa, T. Mitani, *J. Mater. Chem.* **2002**, *12*, 1640.

5 a) S. Fukuzumi, Y. Yoshida, K. Okamoto, H. Imahori, Y. Araki, O. Ito, *J. Am. Chem. Soc.* **2002**, *124*, 6794. b) S. Fukuzumi, K. Okamoto, H. Imahori, *Angew. Chem., Int. Ed.* **2002**, *41*, 620. c) S. Fukuzumi, K. Ohkubo, H. Imahori, J. Shao, Z. Ou, G. Zheng, Y. Chen, R. K. Pandey, M. Fujitsuka, O. Ito, K. M. Kadish, *J. Am. Chem. Soc.* **2001**, *123*, 10676. d) H. Imahori, D. M. Guldi, K. Tamaki, Y. Yoshida, C. Luo, Y. Sakata, S. Fukuzumi, *J. Am. Chem. Soc.* **2001**, *123*, 6617. e) H. Imahori, Y. Sekiguchi, Y. Kashiwagi, T. Sato, Y. Araki, O. Ito, H. Yamada, S. Fukuzumi, *Chem.—Eur. J.* **2004**, *10*, 3184.

6 a) Y. Luo, C. P. Collier, J. O. Jeppesen, K. A. Nielsen, E. DeIonno, G. Ho, J. Perkins, H.-R. Tseng, T. Yamamoto, J. F. Stoddart, J. R. Heath, *ChemPhysChem* **2002**, *3*, 519. b) J. E. Green, J. W. Choi, A. Boukai, Y. Bunimovich, E. Johnston-Halperin, E. DeIonno, Y. Luo, B. A. Sheriff, K. Xu, Y. S. Shin, H.-R. Tseng, J. F. Stoddart, J. R. Heath, *Nature* **2007**, *445*, 414. c) M. Hmadeh, A. C. Fahrenbach, S. Basu, A. Trabolsi, D. Benítez, H. Li, A.-M. Albrecht-Gary, M. Elhabiri, J. F. Stoddart, *Chem.—Eur. J.* **2011**, *17*, 6076.

7 a) C.-T. Chen, *Chem. Mater.* **2004**, *16*, 4389. b) K. Susumu, J. A. N. Fisher, J. Zheng, D. N. Beratan, A. G. Yodh, M. J. Therien, *J. Phys. Chem. A* **2011**, *115*, 5525.

8 a) M. L. H. Green, S. R. Marder, M. E. Thompson, J. A. Bandy, D. Bloor, P. V. Kolinsky, R. J. Jones, *Nature* **1987**, *330*, 360. b) M. Albota, D. Beljonne, J.-L. Brédas, J. E. Ehrlich, J.-Y. Fu, A. A. Heikal, S. E. Hess, T. Kogej, M. D. Levin, S. R. Marder, D. McCord-Maughon, J. W. Perry, H. Röckel, M. Rumi, G. Subramaniam, W. W. Webb, X.-L. Wu, C. Xu, *Science* **1998**, *281*, 1653. c) G. S. He, L.-S. Tan, Q. Zheng, P. N. Prasad, *Chem. Rev.* **2008**, *108*, 1245.

9 a) P. Gütlich, A. Dei, *Angew. Chem., Int. Ed. Engl.* **1997**, *36*, 2734. b) C. G. Pierpont, *Coord. Chem. Rev.* **2001**, *216–217*, 99. c) E. Evangelio, D. Ruiz-Molina, *Eur. J. Inorg. Chem.* **2005**, 2957.

10 a) I. Ratera, D. Ruiz-Molina, F. Renz, J. Ensling, K. Wurst, C. Rovira, P. Gütlich, J. Veciana, *J. Am. Chem. Soc.* **2003**, *125*, 1462. b) G. D'Avino, L. Grisanti, J. Guasch, I. Ratera, J. Veciana, A. Painelli, *J. Am. Chem. Soc.* **2008**, *130*, 12064.

11 a) R. Sakamoto, M. Murata, H. Nishihara, *Angew. Chem., Int. Ed.* **2006**, *45*, 4793. b) R. Sakamoto, S. Kume, H. Nishihara, *Chem.—Eur. J.* **2008**, *14*, 6978. c) M. Hayashi, F. Toshimitsu, R. Sakamoto, H. Nishihara, *J. Am. Chem. Soc.* **2011**, *133*, 14518.

12 a) M. Kurihara, A. Hirooka, S. Kume, M. Sugimoto, H. Nishihara, *J. Am. Chem. Soc.* **2002**, *124*, 8800. b) A. Sakamoto, A. Hirooka, K. Namiki, M. Kurihara, M. Murata, M. Sugimoto, H. Nishihara, *Inorg. Chem.* **2005**, *44*, 7547. c) M.-C. Daniel, A. Sakamoto, J. Ruiz, D. Astruc, H. Nishihara, *Chem. Lett.* **2006**, *35*, 38. d) K. Namiki, A. Sakamoto, M. Murata, S. Kume, H. Nishihara, *Chem. Commun.* **2007**, 4650. e) K. Namiki, M. Murata, S. Kume, H. Nishihara, *New J. Chem.* **2011**, *35*, 2146.

13 a) M. Nihei, M. Kurihara, J. Mizutani, H. Nishihara, *J. Am. Chem. Soc.* **2003**, *125*, 2964. b) R. Sakamoto, M. Murata, S. Kume, H. Sampei, M. Sugimoto, H. Nishihara, *Chem. Commun.* **2005**, 1215. c) R. Sakamoto, S. Kume, M. Sugimoto, H. Nishihara, *Chem.—Eur. J.* **2009**, *15*, 1429.

14 S. Nagashima, M. Murata, H. Nishihara, *Angew. Chem., Int. Ed.* **2006**, *45*, 4298.

15 a) M. Murata, T. Fujita, M. Yamada, M. Kurihara, H. Nishihara, *Chem. Lett.* **2000**, 1328. b) M. Murata, M. Yamada, T. Fujita, K. Kojima, M. Kurihara, K. Kubo, Y. Kobayashi, H. Nishihara, *J. Am. Chem. Soc.* **2001**, *123*, 12903. c) H. Nishihara, M. Murata, *J. Inorg. Organomet. Polym. Mater.* **2005**, *15*, 147. d) M. Kondo, M. Murata, H. Nishihara, E. Nishibori, S. Aoyagi, M. Yoshida, Y. Kinoshita, M. Sakata, *Angew. Chem., Int. Ed.* **2006**, *45*, 5461. e) K. Kojima, W.-w. Zhang, M. Kondo, M. Uchikawa, K. Namiki, T. Fujita, M. Murata, Y. Kobayashi, H. Nishihara, *J. Inorg. Organomet. Polym. Mater.* **2007**, *17*, 135. f) M. Kondo, M. Uchikawa, W.-W. Zhang, K. Namiki, S. Kume, M. Murata, Y. Kobayashi, H. Nishihara, *Angew. Chem., Int. Ed.* **2007**, *46*, 6271. g) M. Kondo, M. Uchikawa, K. Namiki, W.-W. Zhang, S. Kume, E. Nishibori, H. Suwa, S. Aoyagi, M. Sakata, M. Murata, Y. Kobayashi, H.

Nishihara, *J. Am. Chem. Soc.* **2009**, *131*, 12112. h) K. P. Rao, T. Kusamoto, F. Toshimitsu, K. Inayoshi, S. Kume, R. Sakamoto, H. Nishihara, *J. Am. Chem. Soc.* **2010**, *132*, 12472. i) K. P. Rao, T. Kusamoto, R. Sakamoto, Y. Yamamoto, S. Kume, M. Nihei, H. Oshio, H. Nishihara, *Chem. Commun.* **2011**, *47*, 2330. j) K. P. Rao, M. Kondo, R. Sakamoto, T. Kusamoto, M. Nishikawa, S. Kume, M. Nihei, H. Oshio, H. Nishihara, *Chem.—Eur. J.*, in press. doi:10.1002/chem.201101708. k) K. P. Rao, M. Kondo, R. Sakamoto, T. Kusamoto, S. Kume, H. Nishihara, *Chem. Lett.* **2011**, *40*, 1456.

16 a) W. Paw, S. D. Cummings, M. A. Mansour, W. B. Connick, D. K. Geiger, R. Eisenberg, *Coord. Chem. Rev.* **1998**, *171*, 125. b) S. D. Cummings, R. Eisenberg, *Inorg. Chem.* **1995**, *34*, 2007. c) M. Hissler, J. E. McGarrah, W. B. Connick, D. K. Geiger, S. D. Cummings, R. Eisenberg, *Coord. Chem. Rev.* **2000**, *208*, 115. d) W. B. Connick, D. Geiger, R. Eisenberg, *Inorg. Chem.* **1999**, *38*, 3264. e) S. D. Cummings, L.-T. Cheng, R. Eisenberg, *Chem. Mater.* **1997**, *9*, 440. f) S. D. Cummings, R. Eisenberg, *J. Am. Chem. Soc.* **1996**, *118*, 1949. g) J. M. Bevilacqua, R. Eisenberg, *Inorg. Chem.* **1994**, *33*, 2913. h) J. A. Zuleta, J. M. Bevilacqua, R. Eisenberg, *Coord. Chem. Rev.* **1991**, *111*, 237.

17 a) T. K. Maji, K. Uemura, H.-C. Chang, R. Matsuda, S. Kitagawa, *Angew. Chem., Int. Ed.* **2004**, *43*, 3269. b) D. N. Dybtsev, H. Chun, S. H. Yoon, D. Kim, K. Kim, *J. Am. Chem. Soc.* **2004**, *126*, 32. c) M. Dincă, J. R. Long, *J. Am. Chem. Soc.* **2005**, *127*, 9376.

18 a) O. Ohmori, M. Fujita, *Chem. Commun.* **2004**, 1586. b) J. S. Seo, D. Whang, H. Lee, S. I. Jun, J. Oh, Y. J. Jeon, K. Kim, *Nature* **2000**, *404*, 982.

19 R. Matsuda, R. Kitaura, S. Kitagawa, Y. Kubota, R. V. Belosludov, T. C. Kobayashi, H. Sakamoto, T. Chiba, M. Takata, Y. Kawazoe, Y. Mita, *Nature* **2005**, *436*, 238.

20 a) S. Kitagawa, M. Kondo, *Bull. Chem. Soc. Jpn.* **1998**, *71*, 1739. b) O. M. Yaghi, H. Li, C. Davis, D. Richardson, T. L. Groy, *Acc. Chem. Res.* **1998**, *31*, 474. c) T. J. Barton, L. M. Bull, W. G. Klemperer, D. A. Loy, B. McEnaney, M. Misono, P. A. Monson, G. Pez, G. W. Scherer, J. C. Vartuli, O. M. Yaghi, *Chem. Mater.* **1999**, *11*, 2633. d) M. Eddaoudi, D. B. Moler, H. Li, B. Chen, T. M. Reineke, M. O'Keeffe, O. M. Yaghi, *Acc. Chem. Res.* **2001**, *34*, 319. e) N. L. Rosi, M. Eddaoudi, J. Kim, M. O'Keeffe, O. M. Yaghi, *CrystEngComm* **2002**, *4*, 401. f) O. M. Yaghi, M. O'Keeffe, N. W. Ockwig, H. K. Chae, M. Eddaoudi, J. Kim, *Nature* **2003**, *423*, 705. g) S. Kitagawa, R. Kitaura, S.-i. Noro, *Angew. Chem., Int. Ed.* **2004**, *43*, 2334. h) T. Uemura, S. Kitagawa, *Chem. Lett.* **2005**, *34*, 132. i) S. Kitagawa, S.-i. Noro, T. Nakamura, *Chem. Commun.* **2006**, 701. j) J. L. C. Rowsell, O. M. Yaghi, *Angew. Chem., Int. Ed.* **2005**, *44*, 4670. k) S. Kitagawa, K. Uemura, *Chem. Soc. Rev.* **2005**, *34*, 109. l) S. Kitagawa, R. Matsuda, *Coord. Chem. Rev.* **2007**, *251*, 2490. m) S. Kitagawa, *Nature* **2006**, *441*, 584. n) O. M. Yaghi, *Nat. Mater.* **2007**, *6*, 92. o) D. J. Tranchemontagne, J. L. Mendoza-Cortés, M. O'Keeffe, O. M. Yaghi, *Chem. Soc. Rev.* **2009**, *38*, 1257. p) S. Horike, S. Shimomura, S. Kitagawa, *Nat. Chem.* **2009**, *1*, 695. q) J. R. Long, O. M. Yaghi, *Chem. Soc. Rev.* **2009**, *38*, 1213. r) J. Seo, H. Sakamoto, R. Matsuda, S. Kitagawa, *J. Nanosci. Nanotechnol.* **2010**, *10*, 3.

21 a) T. Dewa, K. Endo, Y. Aoyama, *J. Am. Chem. Soc.* **1998**, *120*, 8933. b) K. Uemura, S. Kitagawa, K. Fukui, K. Saito, *J. Am. Chem. Soc.* **2004**, *126*, 3817.

22 T. K. Maji, G. Mostafa, R. Matsuda, S. Kitagawa, *J. Am. Chem. Soc.* **2005**, *127*, 17152.

23 a) C. Hu, U. Englert, *Angew. Chem., Int. Ed.* **2005**, *44*, 2281. b) M. P. Suh, J. W. Ko, H. J. Choi, *J. Am. Chem. Soc.* **2002**, *124*, 10976.

24 J. D. Tovar, T. M. Swager, *J. Org. Chem.* **1999**, *64*, 6499.

25 a) S. Yamaguchi, K. Tamao, *Chem. Lett.* **2005**, *34*, 2. b) S. Yamaguchi, C. Xu, T. Okamoto, *Pure Appl. Chem.* **2006**, *78*, 721. c) A. Fukazawa, S. Yamaguchi, *Chem.—Asian J.* **2009**, *4*, 1386.

26 M. Fakis, J. Polyzos, G. Tsigaridas, J. Parthenios, A. Fragos, V. Giannetas, P. Persephonis, J. Mikroyannidis, *Chem. Phys. Lett.* **2000**, *323*, 111.

